Heliyon 10 (2024) e33845

Contents lists available at ScienceDirect

Heliyon

journal homepage: www.cell.com/heliyon

Research article

The effect of Zn doping on the structure, phase transformation and electric properties of 0.5BZT-0.5BCT materials ☆

Ling Huang [a,b,*]

[a] School of Science, XiJing University, Xi'an, 710123, China
[b] College of Chemistry and Materials, Weinan Normal University, Weinan 714000, China

ARTICLE INFO

Keywords:
Ion doping
Dielectric properties
Ferroelectric phase transformation
Preparation process
High pyroelectricity
BCT-BZT
Sol-gel method

ABSTRACT

In the current study, an improved method of adding Zn ion doping to the 0.5BZT–0.5BCT–based films with high pyroelectric properties was designed. Under different Zn ion doping ratios, the structure, dielectric constant, phase transition relationship and other characteristics of the test product were analyzed experimentally to obtain the optimal ratio parameters. The experimental results demonstrate that the dielectric properties of the 0.5BZT–0.5BCT–xZn–based films proposed in this study can be far superior to those of other films under the optimal preparation process. The optimal dielectric properties and ferroelectric properties are obtained when the doped data are 0.008. Considering the comprehensive dielectric and energy storage capacity, the optimal doping ratio is 0.01, which can take into account dielectric data and energy storage performance. The energy storage density is 1.842 J/cm^3, and the energy storage efficiency exceeds 30%. From 0 to 0.02, the properties of the material, such as the hysteresis loop and phase transition relationship are excellent. The properties of the materials studied in this study are excellent, and they are excellent candidate materials for the future application of ferroelectric materials, and provide ideas for related work.

1. Introduction

Currently, research in energy storage devices is increasingly focused on the development of dielectric capacitors with high energy storage densities [1]. In dielectric capacitors, the dielectric layer stores electrostatic energy in the form of a potential shift caused by an applied electric field, but for current ceramic capacitors the energy storage performance is low and it is difficult to meet the needs of integration, compactness and miniaturization. Thus, the field of dielectric energy storage is increasingly focused on the development of high-energy-storage-density dielectric capacitors.

Generally, the energy storage ceramics include linear dielectric, ferroelectric, antiferroelectric and relaxed ferroelectric. Among the ceramics, the high energy storage density, high energy storage efficiency, and long charge/discharge life cycle of relaxation ferroelectrics make them more suitable for potential applications. The current research related to dielectric materials can be divided into three categories according to the research object: material composition, preparation process, and application requirements of special application scenarios.

☆ This work was supported by Natural Science Foundation of Shaanxi Provincial (No. 2019JQ-922), Natural Science Foundation of Shaanxi Provincial Department of Education (No. 19JK0908), and Weinan Normal University Doctoral Research Launch Fund (No. 2020RC06).

* Correspondence to: School of Science, XiJing University, Xi'an, 710123, China.
E-mail address: huangw2014@163.com.

https://doi.org/10.1016/j.heliyon.2024.e33845
Received 2 April 2024; Received in revised form 25 June 2024; Accepted 27 June 2024

Available online 3 July 2024

The first one is the improvement technique based on the composition of thin film materials. Panupong [2] et al. considered the crystal structure, microstructure, dielectric properties and piezoelectric properties of Mn^{2+}, Mg^{2+}, Nb^{+}, and Cu^{2+} ion doped pairs of BCZT ceramics. He [3] et al. investigated the energy storage performance and efficiency of La doped lead-free relaxation ferroelectric thin film capacitors. Li [4] et al. investigated the properties of composite substrates, made only bilayer LDPE composites, and conducted tests on interfacial polarization, dielectric constant, and so on. Zhu et al. [5] studied the voltage, ferroelectric and dielectric properties of composition gradient BZT–BCT films over a wide temperature range. Kharat et al. [6] studied the synthesis of barium carbonate and its accompanying ternary metal oxide to obtain doping-compliant material methods and properties, and their ferroelectricity, piezoelectricity, and nodal properties are used as a good reference for application requirements. Dash et al. [7] improved the nodal and ferroelectric properties of polymer-ceramic composites by embedding filled particles in the copolymer matrix, which allowed surface hydroxylation. Ibrahim et al. [8] studied the effect of ytterbium metal doping on the ferroelectric properties of lead zirconate and lead zirconate titanate thin films and ceramics prepared by sol-gel method, and showed excellent energy storage properties, which have prospective applications. Fuentes et al. [9] synthesized $BaTiO_3$(BT) nanomaterials by sol–gel combined with the hydrothermal method, and studied the effect of different alkali doping on the ferromagnetic properties of the materials.

The second one is a study based on the improved technique of firing. Reddy [10] et al. tested the excellent energy storage properties of oxygen-treated BCZT films, which can be an excellent candidate for low voltage ferroelectric energy storage materials. Azad [11] et al. performed power delivery simulations using ceramics sintered at different temperatures. Dey et al. [12] focused on the structural property relationships of ceramic materials during polarization and did meticulous comparative experiments and studies. Lin [13] et al. used the pulsed laser deposition technique to confirm the high ferroelectric activity of the material by analyzing the polarized electric field hysteresis lines. Kurokawa et al. [14] investigated the component dependence of polycrystalline BZT–BCT films prepared by combined sputtering. Mondal et al. [15] investigated the use of conventional microwave sintering and hybridized nano-pseudo binary systems synthesized by microwave sintering, which produced more oxygen vacancies in the grain boundary region and effectively improved the dielectric properties of the material. Zhao et al. [16] used the molten salt method to synthesize ultrafine powders for the preparation of BCTZ ceramics. Saparjya et al. [17] focused on the process and finished product properties of BCZT ceramics prepared by the high temperature reaction method. Cakmak et al. [18] prepared lead-free piezoelectric ceramics by dry pressing and strip casting, exhibiting a mixture of normal and relaxed ferroelectric behavior. Hanani et al. [19] conducted studies under hydrothermal conditions and proposed the growth mechanism of the BCZT multipod, which has a certain reference value for the development of complex perovskite oxides. Desoky et al. [20] used mechanical activation to prepare BFBT materials with nanostructured properties, providing important research results for lead-free energy storage applications. Harby et al. [21] prepared BT and Pt-doped glass system materials by the melt quenching method and studied their glass transition behavior, which can be considered effective candidates for various medium power and energy storage applications.

The third one is based on the study of materials technology under special application conditions. Park [22] et al. designed optimized lead-free MME generators for multifunctional energy harvesters based on the power supply needs of electronic medical monitoring devices and smart electronic devices. Maraj et al. [23] noted that perovskite materials are a characteristic dielectric material in the current pulse power capacitor industry and can be used to manufacture devices that efficiently store and supply electrical energy. Sahoo et al. [24] explored lead-free piezoelectric ceramics for practical applications. Hao et al. [25] addressed the issue of the reliability of piezoelectric performance under thermal cycling, which is relevant in practical applications of lead-free piezoelectric materials, by engineering the normal ferroelectric-ferroelectric transition to a diffusive transition. Swain et al. [26] proposed the method of incorporating BZT-BCT into HAp to meet the requirements of the conductive properties of materials required for bone tissue repair. The hardness, toughness and tensile strength of the material can be applied in load-bearing orthopedics and increase the proliferation of human osteogenesis MG63 cells, which have excellent mechanical, electrical and biological properties. The study added significant meaning and value to the application of materials. Barbato et al. [27] focused on highly stable BZT–BCT precursor solutions based on nontoxic and noncarcinogenic solvents. Shin et al. [28] investigated the performance needs of piezoelectric ceramic materials, such as shape based on the application needs of acoustic emission sensors. Roy et al. [29] investigated the effect of porous structure on low-frequency piezoelectric energy harvesting systems and proposed two harvesting systems. Shin et al. [30] designed a porous sandwich structure with a low dielectric constant and a high voltage charge factor for the application of porous sandwich mechanism of BZT–BCT ceramics in energy harvesting. Mansour et al. [31] proposed a nano-humidity sensing material that is tested over a wide humidity range, has the advantages of low hysteresis, excellent repeatability, rapid response and recovery, can be easily coupled with electronic devices, and has strong application capabilities. Amel Mohamed Abouelnaga et al. [32] focused on the application needs of eco-friendly and cost-effective organic–inorganic nanocomposites and prepared ChitosanPEG-Fe_2O_3@NiO nanomagnetic composites with stability, dielectric properties and antibacterial effects.

In the current study, the sol–gel method was used to prepare BZ and BZT15 thin films. The structure, dielectric constant and phase transition relationship of BZT–BCT thin films under different Zn ion doping ratios were analyzed experimentally, and the optimal ratio parameters of ion doping were obtained. The experimental results reveal that the dielectric properties of the 0.5BZT–0.5BCT–xZn–based thin films proposed in this study are far superior to those of other improved methods, and the properties of the hysteresis loop and phase transition relationship are excellent. At the test frequency of 1 MHz, the optimal dielectric properties are achieved when the doping ratio is 0.008. Combining all the test doping ratios, the optimal energy storage efficiency can exceed 55%. Considering the dielectric properties and energy storage properties, it can be considered that the optimal ratio data are 0.01, which have good dielectric properties data under three different test frequencies, energy storage efficiency exceeds 30%, and energy storage density exceeds 1.8 J/cm^3. The zinc-doped BZT–BCT film studied in this study has good performance, and can take into account

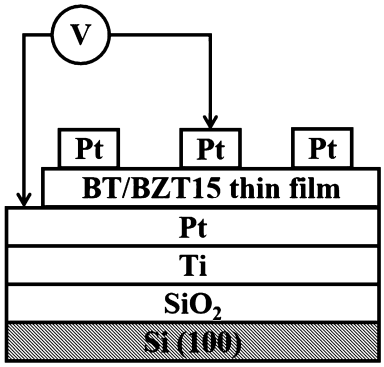

Fig. 1. The configuration of a MFM structure.

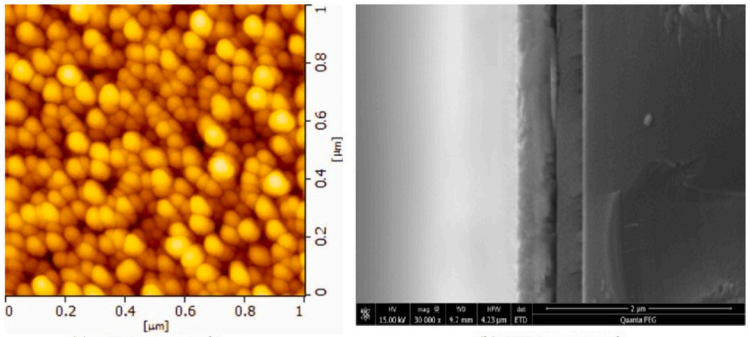

Fig. 2. Scan results of the generated materials. (a) AFM scan result, (b) SEM scan result.

the properties of dielectric constant, dielectric loss, energy storage density and energy storage efficiency, hence, it is a good energy storage material and an excellent candidate material for future ferroelectric material applications.

2. Experimental procedure

BT and BZT15 films were prepared by the sol-gel method. The precursor is a co-solvent composed of $ZnO(CH_3COO)_2$), $TiC_{16}H_{36}O_4$, $Zr(CH_3COO)_4$ and $C_3H_8O_2$. $Ba(CH_3COO)_2$ is initially dissolved in heated acetic acid in predetermined proportions. At room temperature (about 20 °C), $TiC_{16}H_{36}O_4$ and $Zr(CH_3)_4$ were added. Under the above conditions, 2-methoxyethanol is added to ensure that its concentration is not greater than 0.2M. The precursor solution was left for 48 h and rotated at 4200 rpm. The $Pt/Ti/SiO_2$ was deposited on the Si(100) to maintain the structure and properties of the film. The wet film obtained by homogenizing each coating is held at 120 °C for 30 min and heated to 400 °C for 30 min. Finally, after reaching the required thickness, the heat is kept at 800 °C for 15 min. After repeated coating and heat treatment, each performance index reaches 370 nm, and the film with a dense surface and uniform crystal size is obtained.

Thin films were detected by Cu Kα rays ($\lambda = 1.54056$, Eindhoven, Netherlands). The cross-section observation of BZT films was conducted using SEM (Sigma500). In the electrical properties measurement, the film is made into a metal–ferroelectric–metal sandwich, as shown in Fig. 1, and a layer of Pt film is coated on the surface of the film to form a circular tip contact with a diameter of 0.3 cm. The dielectric constant is measured with a high-precision LCR device in the range of 40 Hz–1 MHz. Ferroelectric properties were measured by a precision radiation workstation. The microscopic scanning results are shown in Fig. 2. The surface of the obtained thin film material is dense and uniform, and each layer inside the material is uniform, with a thickness of approximately 60 nm.

3. Results and discussion

3.1. Structural and vibrational analyses

Fig. 3 shows the XRD pattern of the 0.5BZT–0.5BCT–xZn ($0.0 \leq x \leq 0.02$) films at different doping ion ratios, where Figure (a) sets 2θ from 20° to 60°. To analyze the details, the XRD diffraction peaks with 2θ near 45° were fitted together in Figure (b) to plot the relevant detailed data, with the thin solid lines representing the fitted results and the thick solid lines representing the original XRD diffraction peaks.

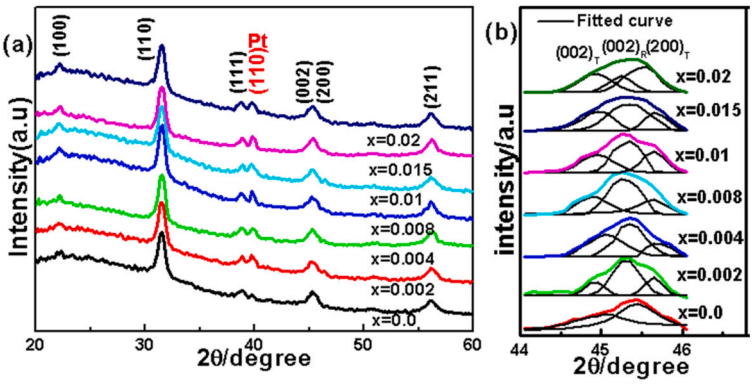

Fig. 3. XRD patterns of films with different doping ratios. (a) 20° - 60°, (b) 45°.

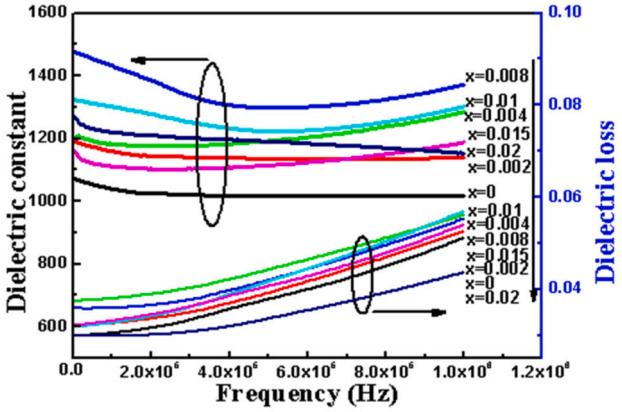

Fig. 4. The dielectric constant and the dielectric loss of films with different doping ratios change with frequency.

As shown in Fig. 3(a), 0.5BZT–0.5BCT–xZn of all experimental proportions showed the same curve trend, without the diffraction characteristic peak of the second phase, forming a stable polycrystalline perovskite structure in the pure phase. This means that Zn ions diffuse into the main phase of 0.5BZT–0.5BCT to form a uniform solid solution.

As shown in Fig. 3(b), all films present three split diffraction peaks near 45°. Compared with the PDF card, these features correspond to the $(002)_T$ and $(200)_T$ diffraction peaks of the tetragonal phase (T phase) and the $(002)_R$ diffraction peaks of the trilateral phase (R phase). Zhao Z.H. et al. [16] also confirmed the coexistence of T-R phases through three split diffraction peaks located at 45°. Concurrently, it can be observed that with an increase in Zn content, the intensity of the $(002)_T/(200)_T/(002)_R$ diffraction peak fluctuates, but it does not show a simple linear relationship. The content ratio of T phase and R phase of Zn ion–doped thin films will change with the change in doping ratio.

3.2. Dielectric property

Fig. 4 shows the variation of dielectric constant εr and dielectric loss $tan\theta$ of the 0.5BZT–0.5BCT–xZn films ($0.0 \leq x \leq 0.02$) with different doping ratios as a function of frequency. The experimental results indicate that the dielectric constant of the film decreases first and becomes stable with an increase in test frequency, while the dielectric loss increases with an increase in the test frequency.

Most researchers believe that the effect of the interface between the film and the bottom electrode on the effective dielectric constant gradually decreases with the increase in thickness. In other words, there are many pinning factors at the interface, and due to the presence of these pinning factors, the motion of the domain walls under the action of small AC electric fields is hindered, especially the domain walls closer to the interface, which are apparently more affected, whereas the domain walls farther away from the interface are relatively less affected. Therefore, the greater the thickness of the film, the more domain walls inside the film that are not affected by the pinning factor at the interface, and the greater the dielectric activity of the film. When studying the dielectric properties of $BaTi_{1-x}Zr_xO_3$ film, Pontes et al. [33] noted that the larger the grain size of the film, the larger the dielectric constant; conversely, the smaller the grain size, the worse the dielectric properties. Ali et al. [34] suggested that a composition structure with two electrochemical activities could further improve electrochemical performance through possible titanium oxide and synergistic effects.

Therefore, the dielectric constant of the film increases with an increase in thickness. An increase in dielectric loss is related to the process of preparing the 0.5BZT–0.5BCT–based films. The thicker the film, the more film spinning and heat treatment it has

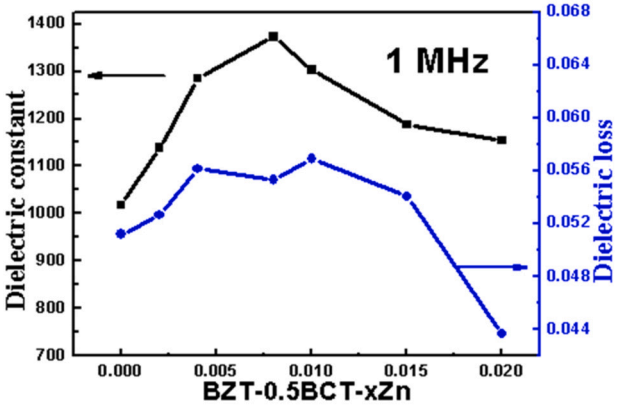

Fig. 5. The dielectric constant and the dielectric loss of Zn-doped films change with the doping ratio.

experienced, and repeated heat treatment tends to cause different film layers to have different shrinkage rates, resulting in thermal stress between adjacent film layers. The more layers of the film, the more defects are formed by thermal stress release, and these defects contain a large number of charge traps. The damping of the flip of the dipole (a), (b) and (c) is macroficially increased, hence, the thicker film shows a larger dielectric loss. In addition, after many experimental tests found that the thickness of the film is too thin, it is difficult to obtain its electrical properties.

Fig. 5 shows the change of dielectric constant εr and dielectric loss $tan\theta$ with the mixing ratio of 0.5BZT–0.5BCT–xZn in the experimental environment of 1 MHz. When x increases from 0 to 0.008, the dielectric constant of the film gradually increases, and the dielectric loss slightly increases. With the further increase of x, dielectric loss and dielectric constant decrease gradually. The experimental results demonstrate that the optimal dielectric properties are obtained when the Zn doping ratio is $x = 0.008$, the dielectric constant $\varepsilon_r = 1372$, and the dielectric loss $tan\theta = 0.055$.

Lin [35] prepared (1-x)BZT–xBCT films of different components by the sol-gel method with dielectric constants ranging from 350 to 500. The dielectric constant of 300 nm thick 0.5BZT-0.5BCT film prepared by Chi [36] is 457. The dielectric constant of 0.5BZT-0.5BCT prepared by Piorra [37] et al. by the PLD method can reach 1010. The dielectric constants of the films obtained in this study are significantly higher than those obtained in these studies, and the dielectric loss data are good. Therefore, a small amount of Zn doping can improve the dielectric properties of the 0.5BZT-0.5BCT films.

3.3. Mesomorphic behavior

To obtain the dielectric constant phase transition behavior of 0.5BZT–0.5BCT–xZn films with different Zn doping ratios ($0.0 \leq x \leq 0.02$), the dielectric constant and dielectric loss of the film materials were tested with a change of temperature, in which the measurement frequency was set at 10 kHz, 100 kHz and 1 MHz. The test temperature ranges from -60 °C to 120 °C, and the measurement results are shown in Fig. 6.

Analysis of the experimental results presented in Fig. 6 shows that the "$\varepsilon_r - T$" curves of all the sample films show a single temperature peak; further, and compared with the sharp temperature peak most commonly presented by ceramic materials, the experimental results reveal a wider temperature peak. This may be related to the fact that the interface and grain size between the $BaTi_{1-x}Zr_xO_3$ film and electrode are smaller than those of ceramic materials [14,36]. It can also be observed that with the increase in Zn content, the mesothermal peak gradually widens, and shows a tendency toward dispersion with the increase in frequency, suggesting that Zn doping in the film shows a ferroelectric behavior characterized by the diffusion phase. Analysis of the "$\varepsilon_r - T$" relationship in the figure shows that dielectric loss is a function of temperature, and in all the experimental results, the value of dielectric loss is small, suggesting that the material has good double electric properties.

3.4. Dielectric properties study

To analyze the phase transition properties of doped films, the dispersion phase transition (DPT) and dispersion characteristics of relaxation ferroelectrics are used.

The ferroelectric–paraelectric phase transition of relaxor ferroelectrics is relatively slow in a certain temperature region, and the mesothermal spectrum shows a wide and slow mesothermal peak at the ferroelectric T–paraelectric C phase transition temperature T_m. The values of phase transition points of the 0.5BZT–0.5BCT–xZn films at different frequencies are shown in Fig. 7. With an increase in Zn content, the phase transition temperature decreases from 60 °C to -20 °C, and the peak of the dielectric constant widens gradually. Concurrently, with an increase in test frequency, under the same doping ratio, the phase transition temperature also shows a certain increase. The change in phase transition temperature shows that the material has DPT behavior.

The dielectric constant and the phase transition temperature of the relaxor ferroelectrics are closely related to the frequency. When $T < T_m$, the dielectric peak and the loss peak at T_m move to the high-temperature direction with an increase in frequency; in other words, as T_m increases with an increase in frequency, the dielectric temperature peak ε_m decreases slightly, but the dielectric loss

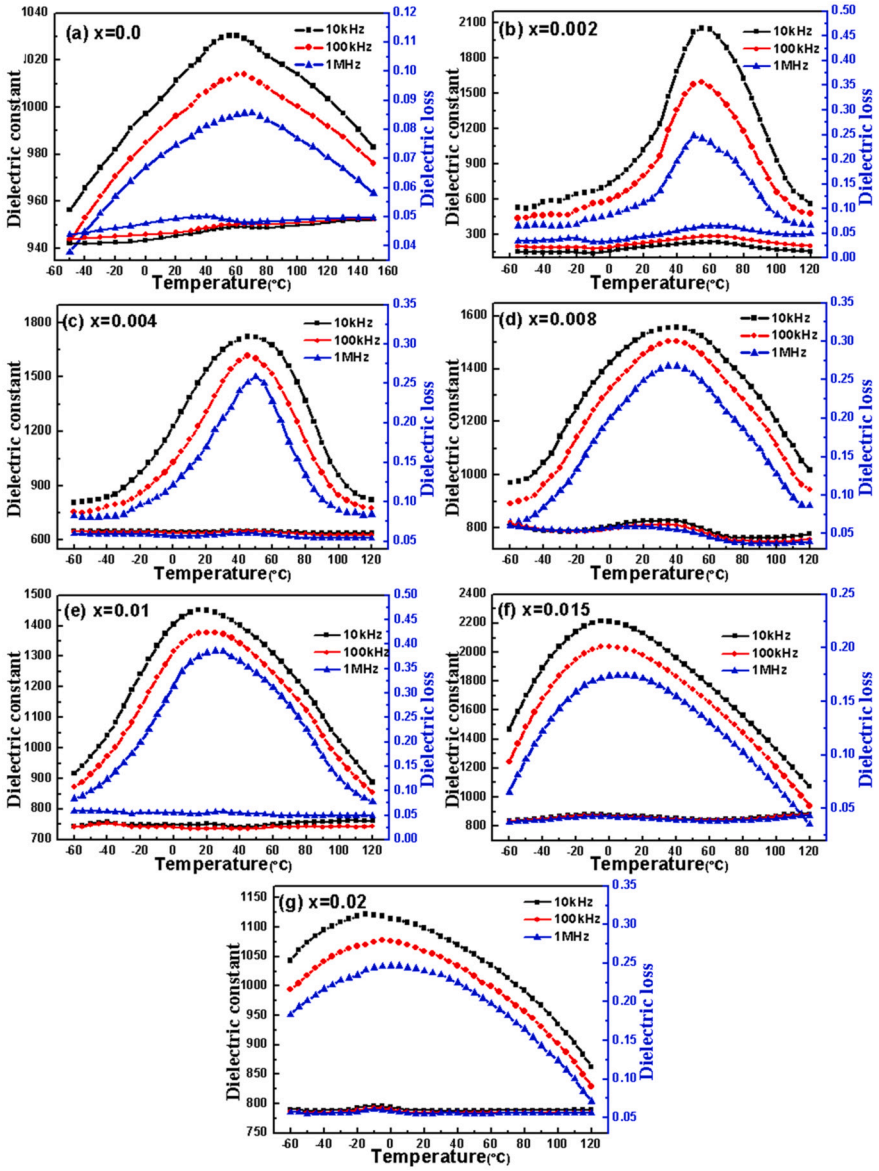

Fig. 6. εr-T and $tan\theta$-T curves of 0.5BZT-0.5BCT-xZn (0.0≤x≤0.02) films. (a) $x = 0.0$, (b) $x = 0.002$, (c) $x = 0.004$, (d) $x = 0.008$, (e) $x = 0.01$, (f) $x = 0.015$, (g) $x = 0.02$.

peak increases slightly. In the temperature region near $T > T_m$, the ε_r–T relation of the relaxor ferroelectrics satisfies the Curie–Weiss square law, as shown in Equation (1) as follows:

$$1/\varepsilon_r - 1/\varepsilon_m = \frac{(T - T_m)^\gamma}{C} \tag{1}$$

where C is the Curie constant; ε_m indicates the dielectric constant corresponding to the dielectric temperature peak; T and ε_r represent, respectively, a specified temperature greater than the Curie temperature and the dielectric constant measured at that temperature; γ represents the dispersion index, suggesting the degree of dispersion of the ferroelectric–paraelectric phase transition. Generally, $1 < \gamma < 2$, $\gamma = 1$ is a traditional ferroelectric, $\gamma = 2$ is a typical relaxation type of ferroelectric, and the closer γ is to 2, the higher the degree of dispersion.

In the above measurements, the dielectric temperature peak of the film broadening deviates from the Curie–Weiss law, showing the characteristics of a diffused ferroelectric-paraelectric phase transition. To further understand the relaxation and DPT behavior of $BaTi_{1-x}Zr_xO_3$ thin films, the natural logarithm of both sides of Formula (1) is calculated to obtain Formula (2).

$$\ln\left(\frac{1}{\varepsilon_r} - \frac{1}{\varepsilon_m}\right) = \gamma \ln(T - T_m) - \ln C' \tag{2}$$

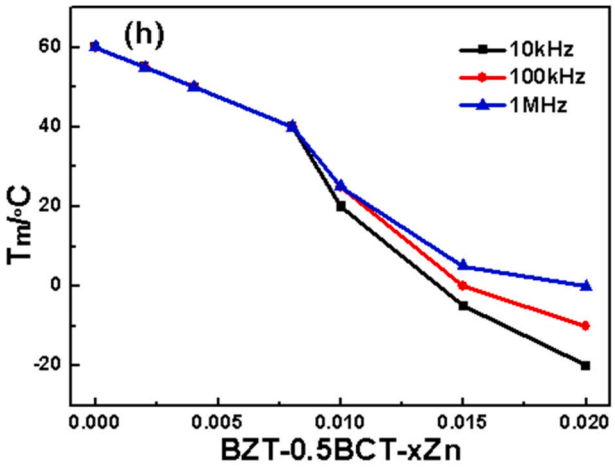

Fig. 7. Tm variation of 0.5BZT-0.5BCT-xZn (0.0≤x≤0.02) films with Zn content.

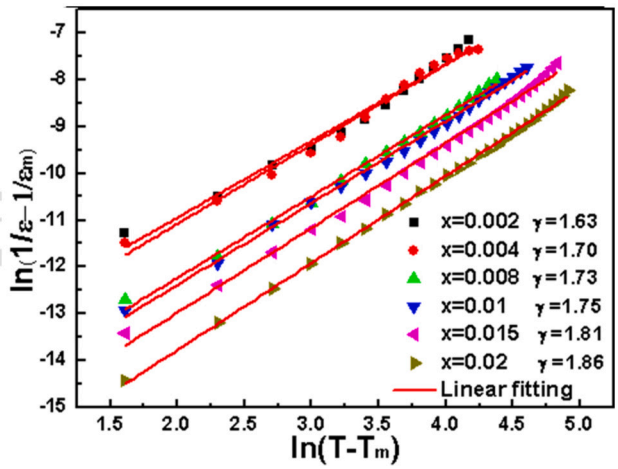

Fig. 8. The relevant experimental results of different Zn doping ratios.

The data are processed according to the formula, the relationship curve of $ln(T - T_m)$ and $ln(1/\varepsilon - 1/\varepsilon_m)$ is drawn, and the linear fitting is conducted. The slope is calculated to obtain the γ value. The relevant experimental results or different Zn doping ratios are shown in Fig. 8.

As shown in Fig. 8, with an increase in Zn content, the γ value increases from 1.63 to 1.86, and all of them are between 1 and 2, which confirms classical ferromagnetism, and indicates that the dispersion of the film gradually increases with an increase in Zn content. This is because Zn^{2+}, as the acceptor ion, occupies the B-site to replace Ti^{4+} or Zr^{4+}, which easily forms an oxygen vacancy. The difference in ionic radii between Zn^{4+} and (Ti^{4+}, Zr^{4+}) and the oxygen vacancy result in a large lattice distortion, which leads to the gradual destruction of the long-range ordered structure with an increase in Zn content. Thus, the domain structure of the material evolves to the nanoscale, and only polar nanoscale regions exist stably under low temperatures and zero-bias electric fields. However, the existence of microregions causes the material to undergo polarization relaxation in a weak field [5].

3.5. Ferroelectric and energy storage investigations

At room temperature, the residual polarization value Pr of the relaxor ferroelectrics is small. The maximum spontaneous polarization Ps is still present in the relaxed ferroelectrics at a temperature above Tm, and the hysteresis loops and electroinduced strain curves can be observed.

Fig. 9 shows the hysteresis loop relationship of the 0.5BZT–0.5BCT–xZn films (0.0≤x≤0.02) with different doping ratios. The polarization values of the 0.5BZT-0.5BCT-xZn films showed a nonlinear increase with an increase in electric field intensity, and a diagonal symmetry relationship with the origin as the axis. The curve presented by the change relationship is a typical hysteresis loop relationship and characteristic; in other words, all the films show well-shaped hysteresis loops; hence, the material energy storage and discharge are lossless, and all the sample films with doping proportions have ferroelectric behavior. Data on the performance, for $x = 0, 0.002, 0.004, 0.008, 0.01, 0.015, 0.02$, in the process of increasing the energy storage density, in turn, is 1.385, 1.390, 0.496,

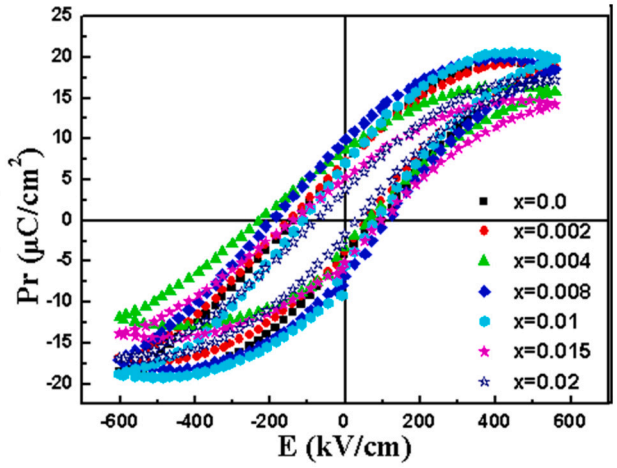

Fig. 9. Hysteresis diagram of.5BZT-0.5BCT-xZn (0.0≤x≤0.02) film.

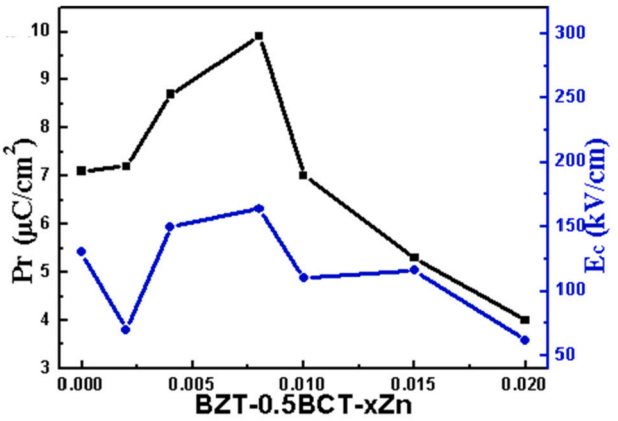

Fig. 10. Changes of P_r and E_c of 0.5BZT-0.5BCT-xZn films with Zn content.

1.166, 1.842, 0.724, 2.707 J/cm^3, energy storage losses, in turn, is 4.129, 3.157, 4.319, 5.022, 4.193, 2.584, 2.173 J/cm^3, and energy storage efficiency of 25.12%, 30.57%, 10.28%, 18.85%, 30.52%, 21.98%, 55.48%.

Fig. 10 shows the variation of polarization value Pr and electric field strength E_c of the 0.5BZT–0.5BCT–xZn thin films with Zn content. With an increase in Zn content, Pr and Ec showed a trend of increasing first and then decreasing.

The phenomenon presented in Fig. 10 is analyzed in combination with the principle.

When $x = 0.0$, that is, without doping, $P_r = 7\mu C/cm^2$ and the $E_c = 130kV/cm$. With an increase of Zn content, when 0.0≤x≤0.008, the film has two phases T and R, and the electric domains in the PPT region where the two ferroelectric phases coexist are more easily flipped, showing a large spontaneous polarization, which enhances the ferroelectric properties of the film. With the further increase of Zn content (x≥0.01), the increased oxygen vacancy will pin the domain switch. In addition, the replacement of Ti^{4+} and Zr^{4+} by Zn doping will narrow the adjacent octahedral void, because the radius of Zn^{2+}(r = 0.74 Å) is larger than that of Ti^{4+}(r = 0.605 Å) and Zr^{4+}(r = 0.72 Å), which will cause the Ti^{4+} or Zr^{4+} in the center of the adjacent octahedron to be difficult to move. Reduce their contribution to polarization, resulting in reduced ferroelectric properties.

The ferroelectric properties of the film are the best at $x = 0.008$, $P_r = 9.9\mu C/cm^2$, $E_c = 164kV/cm$.

4. Conclusion

In the current study, 0.5BZT–0.5BCT films doped with Zn ions were prepared by the sol–gel method. The composition, phase transformation properties, ferroelectric, and dielectric properties of the materials were tested experimentally. XRD analysis shows that the material has three-phase and four-phase properties, and the ratio varies with the doping ratio. The experimental results indicate that the optimal dielectric properties, dielectric constant 1372 and dielectric loss 0.055 are obtained when a doping ratio of 0.008 is selected at the test frequency of 1 MHz. The comprehensive experimental data show that in the energy storage test of doping ratios from 0 to 0.02, doping ratio 0.02 has the optimal energy storage efficiency, energy storage efficiency exceeds 50%, and energy storage density is 1.390J/cm^3, but its dielectric property data performance is poor. The optimal dielectric constant ratio is 0.015, but the energy storage efficiency is only 21.89%, and the energy storage density is only 0.724%. Combining energy storage and

dielectric performance, it can be considered that doping ratio 0.01 is better, energy storage efficiency exceeds 30%, energy storage density is $1.842J/cm^3$, and dielectric data are also higher. The zinc-doped materials designed in this study have good performance in phase transition properties and hysteresis loops, and are excellent candidates for ferroelectric materials in the future. The materials have certain application prospects in piezoelectric materials, nanomechanics, micro-sensors, micro-transformers, and even medical imaging.

CRediT authorship contribution statement

Ling Huang: Writing – review & editing, Writing – original draft, Resources, Project administration, Methodology, Funding acquisition, Formal analysis, Data curation, Conceptualization.

Declaration of competing interest

The authors declare that they have no known competing financial interests or personal relationships that could have appeared to influence the work reported in this paper.

Data availability statement

The relevant data from our study are not published in publicly available databases. And the data will be made available on request.

Acknowledgement

This work was supported by Natural Science Foundation of Shaanxi Provincial (No. 2019JQ-922), Natural Science Foundation of Shaanxi Provincial Department of Education (No. 19JK0908), and Weinan Normal University Doctoral Research Launch Fund (No. 2020RC06).

References

[1] A.P. Sharma, D.K. Pradhan, S.K. Pradhan, M. Bahoura, Large energy storage density performance of epitaxial bct/bzt heterostructures via interface engineering, Sci. Rep. 9 (2019) 16809.
[2] P. Jaiban, T. Theethuan, S. Khumtrong, S. Lokakaew, A. Watcharapasorn, The effects of donor (nb5+) and acceptor (cu2+, zn2+, mn2+, mg2+) doping at b-site on crystal structure, microstructure, and electrical properties of (ba0. 85ca0. 15) zr0. 1ti0. 9o3 ceramics, J. Alloys Compd. 899 (2022) 162909.
[3] S. He, B. Peng, G.J. Leighton, C. Shaw, N. Wang, W. Sun, L. Liu, Q. Zhang, High-performance la-doped bczt thin film capacitors on lanio3/pt composite bottom electrodes with ultra-high efficiency and high thermal stability, Ceram. Int. 45 (2019) 11749–11755.
[4] Z. Liwei, S. Na, W. Xuan, W. Liqiu, C. Haikuo, J. Tianyuan, Analysis on dielectric loss characteristics of polyvinylidene fluoride and its composites, J. Mater. Sci., Mater. Electron. 32 (2021) 26268–26290.
[5] R. Zhu, Z. Wang, Z. Cheng, X. Guo, T. Zhang, Z. Cai, H. Kimura, T. Matsumoto, N. Shibata, Y. Ikuhara, Composition gradient (1-x) ba (zr0. 2ti0. 8) o3-x (ba0. 7ca0. 3) tio3 film with improved dielectric, piezoelectric and ferroelectric temperature stability, Ceram. Int. 46 (2020) 20284–20290.
[6] S.P. Kharat, S.K. Gaikwad, P.G. Nalam, R.C. Kambale, A.R. James, Y.D. Kolekar, C. Ramana, Effect of crystal structure and phase on the dielectric, ferroelectric, and piezoelectric properties of ca2+- and zr4+ -substituted barium titanate, Cryst. Growth Des. 22 (2022) 5571–5581.
[7] S. Dash, V.N. Thakur, A. Kumar, R. Mahaling, S. Patel, R. Thomas, B. Sahoo, D.K. Pradhan, Enhancing functional properties of pvdf-hfp/bzt-bct polymer-ceramic composites by surface hydroxylation of ceramic fillers, Ceram. Int. 47 (2021) 33563–33576.
[8] F. Ibrahim, M. El-Desoky, Exploring ferroelectric properties of sol-gel lead zirconate titanate nano-crystalline thin films and ceramics by doping ytterbium for energy-storage application, Phys. Scr. 98 (2023) 035824.
[9] S. Fuentes, H. Pizarro, P. Gutiérrez, D.E. Díaz-Droguett, N. Barraza, Application of forc distributions to the study of magnetic interactions in co-doped batio3 nanomaterials, Mater. Sci. Eng. B 227 (2018) 39–47.
[10] S.R. Reddy, V.V.B. Prasad, S. Bysakh, V. Shanker, N. Hebalkar, S.K. Roy, Superior energy storage performance and fatigue resistance in ferroelectric bczt thin films grown in an oxygen-rich atmosphere, J. Mater. Chem. C 7 (2019) 7073–7082.
[11] P. Azad, S. Karmakar, A. Kumar, S.M. Ibrahim, R. Vaish, An optimization study on b a 0.85 c a 0.15 z r 0.1 t i 0.9 o 3-based piezoelectric energy-harvester using finite element method, J. Aust. Ceram. Soc. 58 (2022) 309–319.
[12] K. Dey, A. Ahad, K. Gautam, A. Tripathy, S.S. Majid, S. Francoual, C. Richter, M. Singh, A. Sagdeo, E. Welter, et al., Coexistence of local structural heterogeneities and long-range ferroelectricity in pb-free (1- x) ba (zr 0.2 ti 0.8) o 3- x (ba 0.7 ca 0.3) tio 3 ceramics, Phys. Rev. B 103 (2021) L100205.
[13] Q. Lin, D. Wang, B. Luo, R. Ding, D. Lorenzen, S. Li, Composition dependence of ferroelectric and piezoelectric properties of epitaxial (1- x) ba (zr0. 2ti0. 8) o3–x (ba0. 7ca0. 3) tio3 thin films prepared by pulsed laser deposition, Appl. Surf. Sci. 331 (2015) 477–481.
[14] F. Kurokawa, A. Mori, Y. Tsujiura, H. Hida, I. Kanno, Compositional dependence of ba (zr0. 2ti0. 8) o3–(ba0. 7ca0. 3) tio3 piezoelectric thin films prepared by combinatorial sputtering, Thin Solid Films 588 (2015) 34–38.
[15] R. Mondal, P. Mishra, S. Parashar, M. Goswami, Dielectric behaviour of bzt-bct nano pseudobinary system near tcp-assisted morphotopic phase boundary, Ceram. Int. 48 (2022) 12311–12316.
[16] K. Zhao, M. Zheng, X. Yan, M. Zhu, Y. Hou, Effect of direct current and alternating current poling on the piezoelectric properties of ba 0.85 ca 0.15 ti 0.9 zr 0.1 o 3 ceramics, J. Mater. Sci., Mater. Electron. 32 (2021) 27815–27822.
[17] S. Saparjya, T. Badapanda, S. Behera, B. Behera, P.R. Das, Effect of gadolinium on the structural and dielectric properties of bczt ceramics, Phase Transit. 93 (2020) 245–262.
[18] Ö. Çakmak, E. Mensur-Alkoy, G. Toprak, Ö. Tuna, S. Alkoy, Investigation of the electrical properties of textured 0.5 [ba (zr 0.2 ti 0.8)] o 3–0.5 [(ba 0.7 ca 0.3) tio 3] piezoceramics, J. Mater. Sci., Mater. Electron. 31 (2020) 4184–4192.
[19] Z. Hanani, E.h. Ablouh, S. Merselmiz, J. Ghanbaja, D. Mezzane, A. Alimoussa, M. Lahcini, M. Spreitzer, D. Vengust, M. El Marssi, et al., Morphogenesis mechanisms in the hydrothermal growth of lead-free bczt nanostructured multipods, CrystEngComm 23 (2021) 5249–5256.
[20] M. El-Desoky, N. Gazouly, A.E. Hannor, H.A. Yousef, Relaxor multiferroic properties of nanostructured batio3–fe2o3–bi2o3 lead free for energy storage applications, Appl. Phys. A 128 (2022) 1033.

[21] A.E. Harby, A.E. Hannora, M. El-Desoky, Observation of relaxor-like behavior in bt and pt doped glasses for energy storage applications, J. Alloys Compd. 770 (2019) 906–913.
[22] S.H. Park, A. Kumar, J. Kaarthik, V. Annapureddy, J. Ryu, A magneto-mechano-electric generator based on lead-free single-crystal fibers for robust scavenging of ambient magnetic energy, Electro. Mater. Lett. 16 (2020) 369–375.
[23] M. Maraj, W. Wei, B. Peng, W. Sun, Dielectric and energy storage properties of ba (1- x) caxzryti (1- y) o3 (bczt): a review, Materials 12 (2019) 3641.
[24] B. Sahoo, T. Thejas, E. Politova, P. Panda, Effect of dopants on electrical properties of bct-bzt lead free piezo ceramics: a review, Ferroelectrics 582 (2021) 46–62.
[25] Y. Hao, C. Liu, L. He, Y. Ji, L. Zhao, J. Gao, S. Ren, M. Guo, Z. Hou, B. Da, et al., Effect of thermal-cycling on the piezoelectricity of 0.5 ba (zr0. 2ti0. 8) o3-0.5 (ba0. 7ca0. 3) tio3 pb-free piezoceramic, J. Alloys Compd. 847 (2020) 156462.
[26] S. Swain, R. Bhaskar, B. Mishra, M.K. Gupta, S. Dasgupta, P. Kumar, et al., Microstructural, dielectric, mechanical, and biological properties of hydroxyapatite (hap)/bzt-bct (0.5 ba (zr0. 2ti0. 8) o3-0.5 (ba0. 7ca0. 3) tio3) bio-composites with improved mechano-electrical properties for bone repair, Ceram. Int. 48 (2022) 24505–24516.
[27] P.S. Barbato, V. Casuscelli, P. Aprea, R. Scaldaferri, D. Caputo, Optimization of the production process of bzt–bct sol–gel thin films obtained from a highly stable and green precursor solution, Mater. Manuf. Process. 36 (2021) 1642–1649.
[28] D.J. Shin, W.S. Kang, D.H. Lim, B.K. Koo, M.S. Kim, S.J. Jeong, I.S. Kim, Lead-free ae sensor based on bzt–bct ceramics, Sensors 21 (2021) 7100.
[29] A. Roy Chowdhury, N. Saurabh, R. Kiran, S. Patel, Effect of porous auxetic structures on low-frequency piezoelectric energy harvesting systems: a finite element study, Appl. Phys. A 128 (2022) 1–19.
[30] D.J. Shin, D.H. Lim, B.K. Koo, M.S. Kim, I.S. Kim, S.J. Jeong, Porous sandwich structures based on bazrtio3–bacatio3 ceramics for piezoelectric energy harvesting, J. Alloys Compd. 831 (2020) 154792.
[31] A. Mansour, M. Morsy, A.M. El Nahrawy, A.B. Abou Hammad, Humidity sensing using zn (1.6- x) na0. 4cuxtio4 spinel nanostructures, Sci. Rep. 14 (2024) 562.
[32] A.M. Abouelnaga, A. Mansour, A.B. Abou Hammad, A.M. El Nahrawy, Optimizing magnetic, dielectric, and antimicrobial performance in chitosan-peg-fe2o3@ nio nanomagnetic composites, Int. J. Biol. Macromol. 260 (2024) 129545.
[33] F. Pontes, E. Longo, E. Leite, J.A. Varela, Improvement of the dielectric and ferroelectric properties in superlattice structure of pb (zr, ti) o 3 thin films grown by a chemical solution route, Appl. Phys. Lett. 84 (2004) 5470–5472.
[34] A.B.A. Hammad, H.S. Magar, A. Mansour, R.Y. Hassan, A.M.E. Nahrawy, Construction and characterization of nano-oval bati0. 7fe0. 3o3@ nife2o4 nanocomposites as an effective platform for the determination of h2o2, Sci. Rep. 13 (2023) 9048.
[35] Y. Lin, N. Qin, G. Wu, T. Sa, D. Bao, Dielectric relaxor behaviors and tunability of (1- x) ba (zr 0.2 ti 0.8) o 3–x (ba 0.7 ca 0.3) tio 3 thin films fabricated by sol–gel method, Appl. Phys. A 109 (2012) 743–749.
[36] Z.L. Cai, Z.M. Wang, H.H. Wang, Z.X. Cheng, B.W. Li, X.L. Guo, H. Kimura, A. Kasahara, An investigation of the nanomechanical properties of 0.5 ba (ti0. 8zr0. 2) o3–0.5 (ba0. 7ca0. 3) tio3 thin films, J. Am. Ceram. Soc. 98 (2015) 114–118.
[37] A. Piorra, Ferroelektrische Schichten für magnetoelektrische Komposite, Ph.D. thesis, 2014.